IEEE Access
Multidisciplinary | Rapid Review | Open Access Journal

Received January 8, 2020, accepted February 3, 2020, date of publication February 7, 2020, date of current version February 18, 2020.

Digital Object Identifier 10.1109/ACCESS.2020.2972396

Uncertain Frequency Responses of Clamp-Pipeline Systems Using an Interval-Based Method

XUMIN GUO[1], HUI MA[1,2], XUFANG ZHANG[1], ZHUANG YE[1], QIANG FU[1], ZHONGHUA LIU[3], AND QINGKAI HAN[1]

[1]School of Mechanical Engineering and Automation, Northeastern University, Shenyang 110819, China
[2]Key Laboratory of Vibration and Control of Aero-Propulsion System Ministry of Education, Northeastern University, Shenyang 110819, China
[3]Shenyang Engine Research Institute, AECC, Shenyang 110015, China

Corresponding author: Hui Ma (mahui_2007@163.com)

This work was supported in part by the National Natural Science Foundation under Grant 11772089, in part by the Fundamental Research Funds for the Central Universities under Grant N170306004, Grant N170308028, Grant N180708009, and Grant N180306005, in part by the Program for the Innovative Talents of Higher Learning Institutions of Liaoning under Grant LR2017035, and in part by the Liaoning Revitalization Talents Program under Grant XLYC1807008.

ABSTRACT Due to manufacturing errors and material deteriorations in the metal rubber of clamps, the clamp stiffness of the pipeline is uncertain. This paper presents a non-intrusive multi-dimensional Chebyshev polynomial approximation method (M-CPAM) to evaluate uncertain characteristics of the frequency response function (FRF) of the clamp-pipeline system (CPS), where the clamp stiffness parameters are taken as unknown but bounded interval variables. Firstly, a finite element model of the clamp-pipeline system is established. Secondly, the variance-based global sensitivity analysis is implemented to determine significant stiffness parameters. Then, the uncertain intervals of the clamp stiffness are measured by experiments and the dispersion of the clamp stiffness is described. Finally, based on the measured stiffness interval, the uncertain frequency responses of the CPS under different tightening torques are analyzed by the proposed M-CPAM, and the effectiveness of simulation results is verified by experiments. Compared with the results obtained from the Monte Carlo simulation, the experimental measurements, and the polynomial chaos expansion, the proposed M-CPAM provides a more accurate, time-saving and practical method for solving the uncertain frequency responses of the CPS with interval stiffness variables. The results show that the clamp stiffness has great dispersion under the same tightening torque. A frequency shift phenomenon will be observed when the clamp stiffness is uncertain. Moreover, the dispersion of the frequency response of the CPS tends to be concentrated with the increase of the tightening torques.

INDEX TERMS Clamp-pipeline system, experiment, frequency response function, uncertainty analysis, interval-based method.

I. NOMENCLATURE

A	cross-sectional area of the beam element
$\boldsymbol{A}_i$	the i-th order eigenvector
$a_{i_1,\cdots,i_g}$	Chebyshev polynomial expansion coefficient
$\boldsymbol{b}$	uncertain parameter vector
b_i^L, b_i^H	the lower and upper bounds of the ith member of $\boldsymbol{b}$
$\boldsymbol{C}$	damping matrix of the CPS
$\boldsymbol{C}(\boldsymbol{b})$	damping matrix with uncertain interval vector
E	Young's modulus
I	cross-section inertia moment
$\boldsymbol{F}$	external force vector
$f(x_1,\cdots,x_g)$	multi-dimensional Chebyshev polynomial approximation
$f_{\boldsymbol{X}}(\boldsymbol{X})$	joint density of $\boldsymbol{X}$
g	the number of uncertain parameters
$h(x_1,\cdots,x_g)$	actual deterministic frequency response value of CPS
$\boldsymbol{K}_p^e$	stiffness matrix of the beam element
$\boldsymbol{K}_H$	total stiffness matrix of the clamp
$\boldsymbol{K}_P$	stiffness matrix of pipeline
$\boldsymbol{K}$	stiffness matrix of the CPS

The associate editor coordinating the review of this manuscript and approving it for publication was Nagarajan Raghavan.

$\boldsymbol{K}(\boldsymbol{b})$	stiffness matrix with uncertain interval vector
K_x	translational stiffness of the clamp in the x-direction
K_z	translational stiffness of the clamp in the z-direction
$K_{\theta x}$	torsional stiffness of the clamp in the θ_x direction
$K_{\theta z}$	torsional stiffness of the clamp in the θ_z direction
L	length of the beam element
$\boldsymbol{M}$	mass matrix of the CPS
$\boldsymbol{M}_p^e$	mass matrix of the beam element
$\boldsymbol{M}(\boldsymbol{b})$	mass matrix with uncertain interval vector
m	Gaussian points number
n	Chebyshev polynomial expansion number
$\bar{n}$	modal order number
$\hat{n}$	number of stiffness parameters
$\bar{N}$	total number elements of the p-order chaos polynomial set
S_i	primary sensitivity coefficient
S_{Ti}	total sensitivity coefficient
$\boldsymbol{T}_w$	transformation matrix
T_L	tightening torque of the left bolt
T_R	tightening torque of the right bolt
$T_j(x)$	the first-class Chebyshev polynomials
$T_{i_1}(x_1)\cdots T_{i_g}(x_g)$	Chebyshev polynomial value at the interpolation point
$\boldsymbol{u}^e$	node freedom of beam element
$\ddot{\boldsymbol{U}}, \dot{\boldsymbol{U}}, \boldsymbol{U}$	acceleration, velocity and displacement vectors of the CPS
u	the number of zeros appeared in $i_1, \cdots, i_g$
v	beam elements number
V_Y	total variance
V_i, V_{ij}	variance component
$\boldsymbol{X}$	stiffness parameters vector
$\tilde{\boldsymbol{X}}$	tensor product
$\boldsymbol{X}_{-i}$	all parameters of $\boldsymbol{X}$ except X_i
$\boldsymbol{X}_{-ij}$	all parameters of $\boldsymbol{X}$ except X_i and X_j
x_i	standard interval parameter
x_m	Gaussian integral point
ΔF_z	variation of the loading force in the z-direction
Δz	variation of the displacement in the z-direction
ΔT_x	variation of the torque in the θ_x direction

GREEK SYMBOLS

$\Delta\theta_x$	variation of the angular displacement in the θ_x direction
$\rho(x)$	weight function of Chebyshev polynomial
ρ	material density of the pipeline
μ_Y	mean of Y
$\varphi_{\alpha_k}(\zeta_k)$	α_kth-order marginal orthogonal polynomial
δ_{ij}	Kronecker delta symbol

ABBREVIATIONS

FRF	frequency response function
CPS	clamp-pipeline system
MCS	Monte Carlo simulation
PCE	polynomial chaos expansion

II. INTRODUCTION

The pipeline system, as an important component for transporting fluids such as lubricating oil, fuel oil, and hydraulic oil, is widely used in the aviation industry. The pipeline system is fixed on the outside of the engine casing through the clamp [1]. Along with the increasing complexity of working environment, the researches on the vibration of the pipeline system in aero-engines become an important issue. At present, the vibration of the engine external pipeline has become one of the main causes of the aero-engine failure [2], [3]. Meanwhile, the stiffness of the clamp including the metal rubber has inherent uncertainty, which will affect the accurate prediction of the pipeline vibration response. Therefore, it is essential to account for dynamic uncertain characteristics of the CPS and provide an efficient simulation methodology for uncertainty analysis. This paper presents a multi-dimensional Chebyshev polynomial approximation method for uncertain frequency response analysis of the CPS with interval stiffness variables.

The pipeline system, in which the inside diameter of the pipe is much smaller than the pipe length, usually be modeled based on the Euler-Bernoulli beam or the Timoshenko beam model [4]–[9], [26]. Besides, the pipe [10] and the shell element [11], [12] were also used in the literatures to develop the corresponding finite-element model. For instance, Gao et al. established the reduced hydraulic pipeline model using the Euler-Bernoulli beam [6], [7] and Timoshenko beam [8], in which the clamp was simplified as springs. Based on incompressible potential flow, Firouz [12] established a fluid-structure interaction model for stability analysis using the shell model. Quan *et al.* [13] proposed a bionic hydraulic pipeline model based on a vascular physiological structure. And this model includes the rubber material model and the fluid-structure interaction (FSI) dynamic equation. The FSI analysis of an aero hydraulic pipe was carried out by Zhang *et al.* [14], in which various kinds of friction coupling models were compared. Liu and Jiao [15] established a multi-objective pipeline routing algorithm to avoid the possible resonance of aero-engine. Ai *et al.* [16] utilized active control strategies to minimize the pressure-introduced resonance of the hydraulic pipeline. Besides, a variety of constitutive models of the clamp damping material were presented in previous literatures [17]–[19]. Zhang *et al.* [18] established the relationship between the physical parameters (such as the damping factor and the Poisson's ratio of the clamp damping

material) and the preparation parameters, and they found that the mechanical properties of nickel-based rubber can be controlled by adjusting the relative density during manufacturing. Lazutkin *et al.* [19] proposed a novel manufacturing technology to produce the new metal rubber that is more effective than traditional rubber in vibration reduction of pipelines.

The above literatures are about the study of vibration characteristics of deterministic pipeline system. However, the vibration analysis of CPS with uncertainty would be more complex than that of the deterministic models. The uncertainty methods can be roughly divided into three categories: the probabilistic uncertainty method, the fuzzy uncertainty method and the interval uncertainty method [20]. After further considering the uncertain parameters as random or interval variables, a goal of the stochastic vibration analysis is to determine an accurate and robust estimation for response boundaries or the high-order statistical characteristics. In this regard, the method of the polynomial chaos expansion (PCE) has been attracted considerable attention [21]–[30] due to its globally minimized approximation errors. Wan *et al.* [24] proposed a method to deal with a large number of random parameters considering the multi-factor influence of PCE scheme. Manan and Cooper [25] provided regression models for curve fitting of the FRF using the PCE method. Ritto *et al.* [26] used the probabilistic method to consider the uncertain parameters of the internal flow in the pipeline model and extended the stability analysis. Jacquelin *et al.* [28], [29] used the polynomial chaos expansion (PCE) to evaluate a dynamical uncertain system and found the phenomenon of amplitude oscillations in the resonance region. Liu et al. [30] developed a sparse surrogate model for the structural reliability analysis. Zhang *et al.* [31] proposed an efficient sensitivity analysis method using the dimensional reduction algorithm. Dundulis *et al.* [32] proposed an integrated failure probability estimation method to estimate the failure probability of gas pipelines. Duan [33] applied the Monte-Carlo simulation method for uncertainty analysis of pipeline systems with various uncertain pipe and fluid properties. Ahammed and Melchers [34] carried out the probabilistic analysis of pipelines subjected to pitting corrosions. The fuzzy method was investigated in the literatures to model uncertain parameters with ambiguous boundaries or regions [35]–[39]. For instance, Klimke *et al.* [36], [37] used the sparse grid interpolation method to obtain the fuzzy value. Puig *et al.* [38] proposed a solution method for linear systems with fuzzy parameters that do not change with time.

The interval method aims at the uncertain parameters which have clear boundaries but are difficult to describe the distribution. Some typical interval methods include the Taylor series expansion method [40], the polynomial approximation method [20], [41]–[48], etc. Qiu *et al.* [40] applied the Taylor series expansion method to obtain the dynamic response interval of a truss structure. Wu *et al.* [41], [42] illustrated an application of the CPAM for the interval analysis of the two-degree-of-freedom car model. In conjunction with the sparse integration grid, Wu *et al.* [43], [44] improved the numerical efficiency of the Chebyshev inclusion function. Fu et al. [20], [45], [46] applied the interval precise integration method and the Legendre polynomial approximation method for the interval response estimation of cracked rotors. Muscolino *et al.* [47] used the rational series expansion to obtain the interval of the FRF of 24-bar truss structure.

To summarize, Numerical methods for uncertainty analysis have been developed for many engineering models with uncertain parameters. This paper develops a non-intrusive M-CPAM for the uncertain frequency response of clamp-pipeline systems with interval variables, which is seldom studied in previous literatures. Moreover, the intervals of the clamp stiffness are given by experimental tests. And experimental validations of the FRF of the CPS under different tightening torques are carried out, which is a concrete step forward compared with the existing literatures dealing with uncertainty in engineering systems.

The structure of this paper is as follows. Firstly, the establishment of the dynamic model of the clamp-pipeline system and the global sensitivity analysis based on variance are carried out in Section 2. Secondly, the uncertain frequency response analysis method of CPS is proposed in Section 3. Then the effectiveness of the proposed interval-based method is verified by comparing the results of simulation and experiment in Section 4. Finally, the main conclusions are given in Section 5.

III. DYNAMIC MODEL AND PARAMETER SENSITIVITY ANALYSIS OF THE CPS

A. DYNAMIC MODEL OF THE CPS

Euler-Bernoulli beam [6], [7], [26] or Timoshenko beam [8], [9] model is frequently used to calculate the pipeline system whose inner diameter is much smaller than the pipe length. When the ratio between the length and the diameter of the pipeline is greater than 5 times, Euler-Bernoulli beam can be adopted for dynamic modeling [49]. Therefore, the Euler-Bernoulli beam with translational and rotational degrees of freedom in x and z directions is adopted to build the finite element model of the pipeline. This determines a simple simulation model but reserves numerical accuracy in general.

As depicted in Fig 1. (b), each node of the beam model consists of four degrees of freedom. $Oxyz$ is the local coordinate system, and subscripts A and B represent the node A and node B, respectively. In Fig 1. (c), K_x and K_z denote the translational stiffness in the x and z-directions, respectively. $K_{\theta x}$ and $K_{\theta z}$ denote the torsional stiffness in the θx and θz-directions, respectively.

As illustrated in Fig 1(b), each beam element contains the following degrees of freedom:

$$\boldsymbol{u}^e = [x_A, z_A, \theta_{xA}, \theta_{zA}, x_B, z_B, \theta_{xB}, \theta_{zB}]^{\mathrm{T}} \tag{1}$$

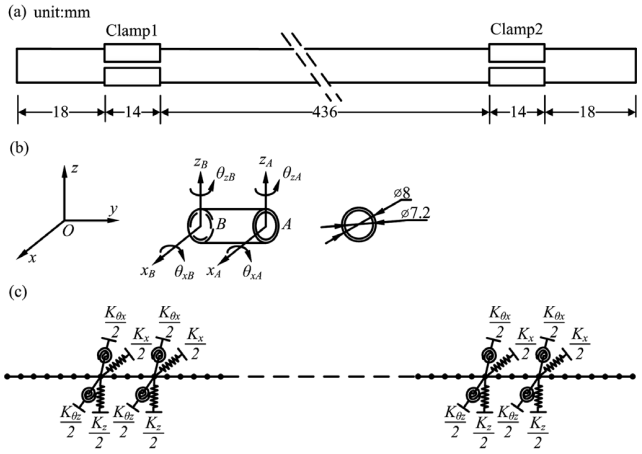

FIGURE 1. The finite-element model of the CPS: (a) physical dimensions, (b) the beam element model, (c) the system finite element model.

and the stiffness matrix can be written as [6]:

$$\boldsymbol{K}_p^e = \frac{EI}{L^3}\begin{bmatrix} 12 & & & & & & & \\ 0 & 12 & & & & & & \\ 0 & -6L & 4L^2 & & & sym & & \\ 6L & 0 & 0 & 4L^2 & & & & \\ -12 & 0 & 0 & -6L & 12 & & & \\ 0 & -12 & 6L & 0 & 0 & 12 & & \\ 0 & -6L & 2L^2 & 0 & 0 & 6L & 4L^2 & \\ 6L & 0 & 0 & 2L^2 & -6L & 0 & 0 & 4L^2 \end{bmatrix} \tag{2}$$

where E is Young's modulus; I is the cross-section inertia moment; L is the length of the beam element.

The mass matrix of the beam element can be expressed as:

$$\boldsymbol{M}_p^e = \frac{\rho AL}{420}\begin{bmatrix} 156 & & & & & & & \\ 0 & 156 & & & & & & \\ 0 & -22L & 4L^2 & & & sym & & \\ 22L & 0 & 0 & 4L^2 & & & & \\ 54 & 0 & 0 & 13L & 156 & & & \\ 0 & 54 & -13L & 0 & 0 & 156 & & \\ 0 & 13L & 3L^2 & 0 & 0 & -22L & 4L^2 & \\ -13L & 0 & 0 & 3L^2 & 22L & 0 & 0 & 4L^2 \end{bmatrix} \tag{3}$$

where ρ is the density; A is the cross-section area.

Considering the influence of the clamp width, the 14mm long clamp is modeled by four springs and four torsional springs (see Fig. 1 (c)). Each spring is set to half of the clamp stiffness. The stiffness matrix of the clamp is expressed as:

$$\begin{aligned} \boldsymbol{K}_H &= \mathrm{diag}\left[0 \cdots \bar{\boldsymbol{K}}_H\ 0 \cdots \bar{\boldsymbol{K}}_H\ 0 \cdots \bar{\boldsymbol{K}}_H\ 0 \cdots \bar{\boldsymbol{K}}_H \cdots 0\right] \\ \bar{\boldsymbol{K}}_H &= \begin{bmatrix} \frac{K_x}{2} & \frac{K_z}{2} & \frac{K_{x\theta}}{2} & \frac{K_{z\theta}}{2} \end{bmatrix} \end{aligned} \tag{4}$$

The global stiffness matrix and mass matrix of the pipeline can be written as $\boldsymbol{K_p}$ and $\boldsymbol{M}$.

$$\boldsymbol{K}_p = \sum_{w=1}^{v} \boldsymbol{T}_w^{\mathrm{T}} K_p^{ew} \boldsymbol{T}_w, \quad \boldsymbol{M} = \sum_{w=1}^{v} \boldsymbol{T}_w^{\mathrm{T}} \boldsymbol{M}_p^{ew} \boldsymbol{T}_w \tag{5}$$

where v is the number of beam elements; $\boldsymbol{K}_p^{ew}$ denotes the extended matrix of the w-th mass element matrix; $\boldsymbol{M}_p^{ew}$ denotes the extended matrix of the w-th stiffness element matrix. $\boldsymbol{T}_w$ represents the transformation matrix. The model established in this paper is a straight pipe model, so $\boldsymbol{T}_w$ is the unit matrix.

The total stiffness matrix of the CPS is:

$$\boldsymbol{K} = \boldsymbol{K}_p + \boldsymbol{K}_H \tag{6}$$

and the Rayleigh damping is considered:

$$\begin{cases} \boldsymbol{C} = \alpha \boldsymbol{M} + \beta \boldsymbol{K} \\ \alpha = 4\pi(\xi_2/\omega_2 - \xi_1/\omega_1)/\left(1/\omega_2 - 1/\omega_1\right) \\ \beta = (\xi_2\omega_2 - \xi_1\omega_1)/\left(\omega_2^2 - \omega_1^2\right) \end{cases} \tag{7}$$

where $\omega_1 = 2\pi f_1$ and $\omega_2 = 2\pi f_2$; f_1 and f_2 denote the first two-order natural frequencies; $\xi_1 = 0.02$ and $\xi_2 = 0.02$ are the modal damping ratios of the CPS. This determines the equation of motion for the CPS can be written as:

$$\boldsymbol{M}\ddot{\boldsymbol{U}} + \boldsymbol{C}\dot{\boldsymbol{U}} + \boldsymbol{K}\boldsymbol{U} = \boldsymbol{F} \tag{8}$$

where $\boldsymbol{M}$is the mass matrix, $\boldsymbol{C}$is the damping matrix, $\boldsymbol{F}$ is the external force vector. $\ddot{\boldsymbol{U}}$, $\dot{\boldsymbol{U}}$ and $\boldsymbol{U}$ is the acceleration, velocity and displacement vectors of the CPS, respectively.

The displacement transfer function matrix of the CPS is written as:

$$\boldsymbol{H}_d(\omega) = (-\boldsymbol{M}\omega^2 + \mathrm{j}\omega\boldsymbol{C} + \boldsymbol{K})^{-1} \tag{9}$$

Following the orthogonality of vibration modes, Eq. (9) can be further rewritten as [50]:

$$\boldsymbol{H}_d(\omega) = \sum_{i=1}^{\bar{n}} \frac{\boldsymbol{A}_i \boldsymbol{A}_i^{\mathrm{T}}}{-\omega^2 + 2\xi_i\omega_i\mathrm{j}\omega + \omega_i^2} \tag{10}$$

where $\boldsymbol{A}_i$ and ω_i are the i-th order eigenvector matrix and eigenvalue, respectively, and ξ_i is the i-th modal damping ratio, $\bar{n}$ is the modal order number.

This further determines the transfer function matrix for the structural acceleration as:

$$\boldsymbol{H}_a(\omega) = \sum_{i=1}^{\bar{n}} \frac{-\omega^2 \boldsymbol{A}_i \boldsymbol{A}_i^{\mathrm{T}}}{\omega_i^2 + 2\xi_i\omega_i\mathrm{j}\omega - \omega^2} \tag{11}$$

The acceleration frequency response function of the excitation point $\hat{a}$ and the measurement point $\hat{b}$ is:

$$H_a^{\hat{a}\hat{b}}(\omega) = \sum_{i=1}^{\bar{n}} \frac{-\omega^2 A_{\hat{a}i} A_{\hat{b}i}}{\omega_i^2 + 2\xi_i\omega_i\mathrm{j}\omega - \omega^2} \tag{12}$$

where $A_{\hat{a}i}$ and $A_{\hat{b}i}$ represent the values at points $\hat{a}$ and $\hat{b}$ in the eigenvector of the i-th order.

B. THE GLOBAL SENSITIVITY ANALYSIS OF THE CPS

The clamp is composed of the strap, metal rubber and connecting bolt. As a matter of fact, due to manufacturing errors and material deteriorations in the metal rubber, the stiffness of the clamp is naturally uncertain. In order to study the effect of the uncertainty of clamp stiffness on the system, sensitivity analysis is necessary first. The frequency equation of the CPS can be generally represented by a multivariate function $Y = h(\boldsymbol{X})$. Herein, the vector $\boldsymbol{X}$ containing all stiffness parameters K_x, K_z, $K_{\theta x}$, and $K_{\theta z}$ is used to mimic the dynamic characteristic of clamps. To identify significant stiffness parameters, the variance-based global sensitivity analysis is employed as follows:

$$h(\boldsymbol{X}) = \mu_Y + \sum_{k=1}^{\hat{n}} h_i\left(\boldsymbol{X}_i\right) + \sum_{i<j} h_{ij}\left(X_i, X_j\right) + \sum_{i<j<k} h_{ijk}\left(X_i, X_j, X_k\right) + \cdots + h_{12\cdots\hat{n}}(\boldsymbol{X}) \quad (13)$$

where μ_Y denotes the mean of Y. $\hat{n}$ represents the number of stiffness parameters. The component functions are defined as:

$$\begin{cases} h_i\left(X_i\right) = E_{-i}\left[h(\boldsymbol{X})|X_i\right] - \mu_Y \\ h_{ij}\left(X_i, X_j\right) = E_{-ij}\left[h(\boldsymbol{X})|X_i, X_j\right] - h_i\left(X_i\right) \\ \qquad\qquad - h_j\left(X_j\right) - \mu_Y (\forall j > i) \\ \cdots \end{cases} \quad (14)$$

in which, the conditional expectations $E_{-i}\left[h(\boldsymbol{X})|X_i\right]$ and $E_{-ij}\left[h(\boldsymbol{X})|X_i, X_j\right]$ are [31]:

$$\begin{cases} E_{-i}[h(\boldsymbol{X})|X_i = x_i] = \int_{\boldsymbol{X}_{-i}} h(\boldsymbol{X}_{-i}, x_i) f_{\boldsymbol{X}_{-i}}(\boldsymbol{X}_{-i}) \mathrm{d}\boldsymbol{X}_{-\mathrm{i}} \\ E_{-ij}[h(\boldsymbol{X})|X_i = x_i, X_j = x_j] \\ = \int_{\boldsymbol{X}_{-ij}} h(\boldsymbol{X}_{-ij}, x_i, x_j) f_{\boldsymbol{X}_{-ij}}(\boldsymbol{X}_{-ij}) \mathrm{d}\boldsymbol{X}_{-\mathrm{ij}} \quad (\forall j > i) \\ \cdots \end{cases} \quad (15)$$

This implies the sub-vector $\boldsymbol{X}_{-i}$ of ($\hat{n}$-1) parameters contain all elements of $\boldsymbol{X}$ except X_i, whereas $\boldsymbol{X}_{-ij}$ is a vector of ($\hat{n}$-2) parameters without X_i and X_j. $f_{\boldsymbol{X}}(\boldsymbol{X})$ is the joint density of $\boldsymbol{X}$. Especially, the conditional expectations in Eq. (15) are equal to the expected value of $h(\boldsymbol{X})$ itself:

$$\begin{aligned} &E_i\{E_{-i}[h(\boldsymbol{X})|X_i]\} = \mu_Y, \\ &E_{ij}\{E_{-ij}[A(\boldsymbol{X})|X_i, X_j]\} = \mu_Y, \\ &\cdots \end{aligned} \quad (16)$$

Therefore, the total variance of $h(\boldsymbol{X})$ can be orthogonally decomposed as:

$$V_Y = \sum_{i=1}^{\hat{n}} V_i + \sum_{i<j} V_{ij} + \sum_{i<j<k} V_{ijk} + \cdots \quad (17)$$

where the variance components are defined as:

$$V_i = E_i[h_i^2(X_i)],\ V_{ij} = E_{ij}[h_{ij}^2(X_i, X_j)], \cdots \quad (18)$$

In which, V_i is referred to as primary effect. V_{ij} denotes the effect of interaction between X_i and X_j on V_Y. The variance component V_i is interpreted as the expected reduction of the total variance V_Y obtained as a result of fixing X_i, which derives the primary sensitivity coefficient of stiffness parameter X_i as follows:

$$S_i = \frac{V_i}{V_Y} = \frac{E_i[h_i^2(X_i)]}{V_Y} \quad (19)$$

According to this definition, all sensitivity indices can be expressed, and added up to one:

$$\sum_{i=1}^{\hat{n}} S_i + \sum_{i<j} S_{ij} + \sum_{i<j<k} S_{ijk} + \cdots + S_{12\cdots\hat{n}} = 1 \quad (20)$$

The total sensitivity focuses on the reduction in variance should all input variables but $\mathbf{X}_i$ be fixed. This reduction in variance is written as $V_{-i}\left[E_i(Y|\boldsymbol{X}_{-i})\right]$. And the remaining variance of Y after fixing X_i is expressed as:

$$V_{Ti} = V_Y - V_{-i}\left[E_i\left(Y|\boldsymbol{X}_{-i}\right)\right] \quad (21)$$

In view of the identity of total variance, $V_Y = V_{-i}\left[E_i\left(Y|\boldsymbol{X}_{-i}\right)\right] + E_{-i}\left[V_i\left(Y|\boldsymbol{X}_{-i}\right)\right]$, the total sensitivity coefficient can be written as:

$$S_{Ti} = \frac{V_Y - V_{-i}\left[E_i\left(Y|\boldsymbol{X}_{-i}\right)\right]}{V_Y} = \frac{E_{-i}\left[V_i\left(Y|\boldsymbol{X}_{-i}\right)\right]}{V_Y} \quad (22)$$

In order to easily illustrate the effect of the uncertainty of clamp stiffness on the CPS, the low-frequency region that contains the first and second-order frequencies of the CPS are selected for uncertainty analysis in this paper. The parameters of the CPS are as follows: Young's modulus, density and Poisson's ratio of pipeline are 204 GPa, 7850 kg/m^3 and 0.3, respectively. The length, inner diameter and outer diameter of pipeline are 500 mm, 6.4 mm and 8 mm, respectively.

The pipeline is fixed on the casing. When the casing has a large vibration displacement, the vibration excitation is transmitted to the pipeline through the clamp. The thin-walled casing mainly suffers from radial deformation, so the pipeline fixed on the casing is mainly subject to external radial excitation. Therefore, the uncertain acceleration frequency response of the pipeline system in the z-direction (radial direction) is the main object of this paper. The sensitivity of the spring variable can be quantified by the contribution of the variable to the total variance of the frequency equation. Thus, the global sensitivity of CPS is analyzed by Monte Carlo simulation. Assuming that the spring stiffness conforms to the normal distribution, the mean stiffness of clamp in four directions is the same as those in Ref. [51]. The variable coefficient of the spring parameters is set as 0.1. The sensitivity analysis results with 10000 samples are shown in Figs. 2 and 3.

The primary sensitivity mainly considers the influence of a single input variable on the system output. While the total sensitivity includes not only the effects of changes in a single input variable on the system, but also the effects of interactions with other input variables on the system output. The difference between the total sensitivity and the primary

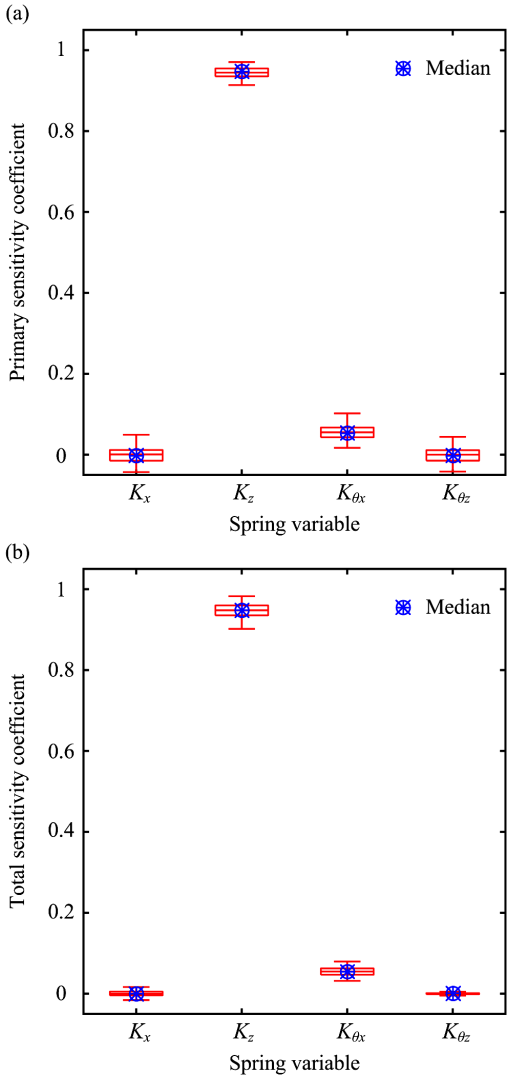

FIGURE 2. Global sensitivity coefficients of four spring parameters to the first-order frequency of the CPS: (a) primary sensitivity coefficient, (b) total sensitivity coefficient. Each boxplot is determined by 100 rounds of the MCS method.

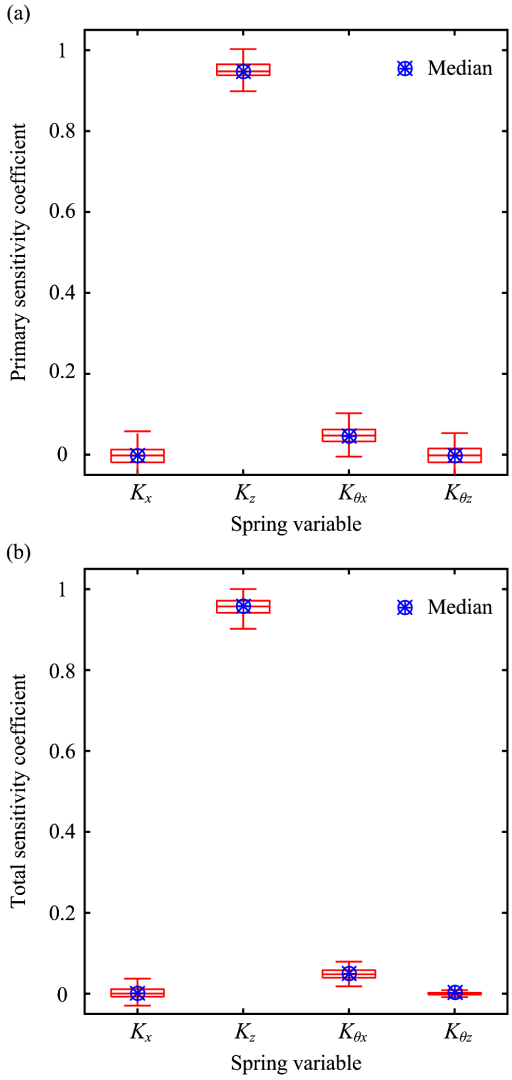

FIGURE 3. Global sensitivity coefficients of four spring parameters to the second-order frequency of the CPS: (a) primary sensitivity coefficient, (b) total sensitivity coefficient. Each boxplot is determined by 100 rounds of the MCS method.

sensitivity can be used to measure the coupling effect of a single spring with other springs. In Fig. 2, the primary sensitivity coefficients of K_z and $K_{\theta x}$ are 0.9344 and 0.0553, respectively. And the total sensitivity coefficients of K_z and $K_{\theta x}$ are 0.9378 and 0.0568, respectively. In Fig. 3, the primary sensitivity coefficients of K_z and $K_{\theta x}$ are 0.9417 and 0.0473, respectively. And the total sensitivity coefficients of K_z and $K_{\theta x}$ are 0.9473 and 0.0480, respectively. Results show that the total sensitivity of the first and second-order frequencies of CPS is slightly greater than the main sensitivity, which indicates that the coupling effect of springs could be ignored. The changes of K_z and $K_{\theta x}$ springs dominate, whereas the sensitivity coefficients of the other two spring parameters (K_x and $K_{\theta z}$) are approximately 0. Therefore, the uncertainty caused by the changes of K_z and $K_{\theta x}$ will be the focus of this paper.

IV. METHODS FOR UNCERTAIN FREQUENCY RESPONSE ANALYSIS OF THE CPS

The structure of this section is as follows. Firstly, the Polynomial chaos expansion (PCE) method is briefly introduced in Section 3.1. Then a multi-dimensional Chebyshev polynomial approximation method based on interval algorithm is proposed in Section 3.2. Finally, aiming at CPS, in order to illustrate the advantages of the interval method proposed in this paper over other methods (PCE and MCS), the results of the two examples calculated by the three methods will be compared in Section 3.3. Among them, Monte Carlo simulation (MCS), as a common method, will not be repeated here.

A. POLYNOMIAL CHAOS EXPANSION METHOD

A commonly used probability method (PCE) is briefly introduced. Firstly, define an index vector $\alpha = [\alpha_1, \cdots, \alpha_{\hat{n}}]^{\mathrm{T}}$ with

each integer $\alpha_i \in [0, p]$. Then, the order of a $\hat{n}$-variate chaos polynomial $\varphi_{\boldsymbol{\alpha}}(\boldsymbol{X})$ can be expressed using the length of the index vector $|\alpha| = \sum_{k=1}^{\hat{n}} \alpha_k$. On this basis, a set of chaos polynomials is defined by using the highest order-parameter p and $\hat{n}$-dimensional random vector X can be written as:

$$\{\phi_i(\boldsymbol{X}), i = 0, \cdots, \bar{N}-1\} := \bigcup_{|\boldsymbol{\alpha}| \le p} \prod_{k=1}^{\hat{n}} \varphi_{\alpha_k}(X_k) \quad (23)$$

where $\varphi_{\alpha_k}(X_k)$ denotes an α_kth-order marginal orthogonal polynomial represented uniquely by the probabilistic characteristic of the input random variable X_k.

It is worth noting that the number of elements of the p-order chaos polynomial set $\{\phi_i(\boldsymbol{X})\}_{i=0}^{\bar{N}-1}$ is:

$$\bar{N} = \binom{\hat{n}+p}{p} = \frac{(\hat{n}+p)!}{\hat{n}!p!} \quad (24)$$

where p is the highest polynomial order and $\hat{n}$ is the dimensionality of the input random vector $\boldsymbol{X}$. In addition, arbitrary two elements in the polynomial set $\{\phi_i(\boldsymbol{X}), i = 0, \cdots, \bar{N}-1\}$ are orthogonally defined. And $E\left[\phi_i(\boldsymbol{X}), \phi_j(\boldsymbol{X})\right] = \delta_{ij}$ (as $i, j = 0, \cdots, \bar{N}$), where δ_{ij} is the Kronecker delta symbol.

On the basis of the generalized Fourier expansion theorem, the original FRF $H(\boldsymbol{X}; \omega)$ can be approximately represented by the polynomial chaos expansion (PCE) basis functions with $\bar{N}$ terms:

$$\hat{H}(\boldsymbol{X}; \omega) = \sum_{i=0}^{\bar{N}-1} a_i(\omega)\phi_i(\boldsymbol{X}) \quad (i = 0, \cdots, \bar{N}-1) \quad (25)$$

where $\hat{H}(\boldsymbol{X}; \omega)$ is the approximation model. The expansion coefficients $a_i(\omega)$ are evaluated as:

$$a_i(\omega) = \int_{\boldsymbol{X}} \phi_i(\boldsymbol{X}) H(\boldsymbol{X}; \omega) f_{\boldsymbol{X}}(\boldsymbol{X}) \mathrm{d}\boldsymbol{X} \quad (i = 0, \cdots, \bar{N}-1) \quad (26)$$

The PCE surrogate model could obtain a good approximation of the original FRF $H(\boldsymbol{X}; \omega)$, given that:

$$\lim_{\bar{N} \to +\infty} \Pr\left[\left\| H(\boldsymbol{X}; \omega) - \sum_{i=0}^{\bar{N}-1} a_i \phi_i(\boldsymbol{X}) \right\|_2 = 0 \right] = 1 \quad (27)$$

where $\| \cdot \|_2$ represents the Euclidian norm for the residual error function of the $\bar{N}$-term-based PCE surrogate model. $\Pr[\cdot]$ denotes the probability. The detailed derivation process of PCE can be found in Ref. [30].

B. THE PROPOSED MULTI-DIMENSIONAL CHEBYSHEV POLYNOMIAL APPROXIMATION METHOD

In view of the spring stiffness of the two clamps on the left and right sides of the pipeline in the same direction is not exactly the same, the one-dimensional Chebyshev polynomial approximation method which can only consider the variation of one parameter in the estimation of frequency response function may not be appropriate. Therefore, a multi-dimensional Chebyshev polynomial approximation method (M-CPAM) that belongs to an interval algorithm is proposed. The uncertain parameter vector can be written as:

$$\boldsymbol{b} = [b_1, b_2, \cdots b_g], \quad b_i \subset [b_i^L, b_i^H] \quad (i = 1, 2, \cdots g) \quad (28)$$

where g is the number of uncertain parameters, b_i^L and b_i^H are the lower and upper bounds of the i-th element of b, respectively.

Before introducing the interval algorithm, the basic principle and steps of function approximation based on Chebyshev orthogonal polynomial are briefly introduced. The first-class Chebyshev polynomials can be written as:

$$T_j(x) = \cos(j \arccos(x)), \quad x \in [-1, 1] \quad (29)$$

$$\begin{cases} T_0(x) = 1 \\ T_1(x) = x \\ T_{j+1}(x) = 2xT_j(x) - T_{j-1}(x), \quad j = 1, 2, \cdots, n \end{cases} \quad (30)$$

where n is the order of the Chebyshev polynomial. This Chebyshev polynomial is orthogonal with the weight function $\rho(x) = \frac{1}{\sqrt{1-x^2}}$

$$\int_{-1}^{1} \frac{T_i(x)T_j(x)}{\sqrt{1-x^2}} \mathrm{d}x = \begin{cases} \pi & i = j = 0 \\ \pi/2 & i = j \neq 0 \\ 0 & i \neq j \end{cases} \quad (31)$$

According to Weierstrass theorem, a polynomial function $f(x)$ can always be found that satisfies the following formula:

$$\|h(x) - f(x)\| \le \varepsilon \quad (32)$$

where ε is any small positive real number, $h(x)$ is the original function.

The Chebyshev polynomial approximation function is defined in the standard interval $[-1, 1]$, whereas the uncertain clamp stiffness is arbitrary interval. Therefore, the interval transformation should be used to convert the arbitrary interval $[b_i^L, b_i^H]$ into the standard interval $[-1, 1]$.

$$x_i = \frac{2b_i - b_i^H - b_i^L}{b_i^H - b_i^L}, \quad x_i \in [-1,\ 1],\ b_i \in \left[b_i^L,\ b_i^H\right] \quad (33)$$

Extending to multiple dimensions, an n-order optimal square approximation on the basis of the Chebyshev orthogonal polynomials is established. The multi-dimensional Chebyshev polynomial approximation $\mathrm{f}(x_1, \cdots, x_g)$ can be expressed as:

$$\begin{aligned} \mathrm{h}(x_1, \cdots, x_g) &\approx \mathrm{f}(x_1, \cdots, x_g) \\ &= \sum_{i_1=0}^{n} \cdots \sum_{i_g=0}^{n} \left(\frac{1}{2}\right)^u a_{i_1, \cdots, i_g} T_{i_1}(x_1) \cdots T_{i_g}(x_g) \end{aligned} \quad (34)$$

where u denotes the number of zeros appeared in $i_1, \cdots, i_g$; $a_{i_1,\cdots,i_g}$ represents the Chebyshev polynomial expansion coefficient, which can be written as:

$$a_{i_1,\cdots,i_g} = \left(\frac{2}{\pi}\right)^g \int_{-1}^{1} \cdots \int_{-1}^{1} \times \frac{h(x_1,\cdots,x_g)T_{i_1}(x_1)\cdots T_{i_g}(x_g)}{\sqrt{1-x_1^2}\cdots\sqrt{1-x_g^2}} \mathrm{d}x_1 \cdots \mathrm{d}x_g \quad i_1,\cdots,i_g = 0,1,2\cdots \tag{35}$$

Since the original frequency response function is usually complex in form, it is difficult to integrate directly. Converting the multiple integral of Eq. (35) into a numerical integral, and then the polynomial coefficient $a_{i_1,\cdots,i_g}$ can be calculated by Gauss-Chebyshev numerical integral.

$$a_{i_1,\cdots,i_g} = \left(\frac{2}{h}\right)^g \sum_{i_1=1}^{m} \cdots \sum_{i_g=1}^{m} h(x_1,\cdots,x_g)T_{i_1}(x_1)\cdots T_{i_g}(x_g) = \left(\frac{2}{h}\right)^g \sum_{i_1=1}^{m} \cdots \sum_{i_g=1}^{m} R(\tilde{\boldsymbol{X}}) \tag{36}$$

where $R(\tilde{\boldsymbol{X}}) = R(x_1,\cdots,x_g) = \sum_{i_g=1}^{m} h(x_1,\cdots,x_g)T_{i_1}(x_1)\cdots T_{i_g}(x_g)$.

$h(x_1,\cdots,x_g)$ and $T_{i_1}(x_1)\cdots T_{i_g}(x_g)$ represent the actual deterministic frequency response value and the Chebyshev polynomial value at the interpolation point. $\tilde{\boldsymbol{X}} \in (x_1^1,\cdots,x_m^1)\otimes\cdots\otimes(x_1^g,\cdots,x_m^g)$ denotes the tensor product of the Gaussian point. It is worth noting that the number of the symbol $\otimes$ is $g-1$. The number of Gaussian points on each dimension is $m(m \geq n+1)$. For Chebyshev type Gaussian integral, the Gaussian integral point can be denoted as:

$$x_m = \cos\left(\frac{2m-1}{k}\pi\right), \quad k = 1,2,\cdots,m \tag{37}$$

In this way, the polynomial coefficients $a_{i_1,\cdots,i_g}$ can be determined by the original function value and the Chebyshev polynomial function value at the Gaussian interpolation points. By substituting Eq. (36) into Eq. (34), the Chebyshev polynomial surrogate model of the frequency response function can be obtained.

According to the above sensitivity analysis result, K_z, and $K_{\theta x}$ have a great influence on the uncertainty analysis of CPS. Thus, g is taken as 4 in Eq. (34), that is, K_{z1}, K_{z2}, $K_{\theta x1}$, and $K_{\theta x2}$ are interval variables. And the uncertain parameter vector can be specifically expressed as:

$$\boldsymbol{b} = [b_1, b_2, b_3, b_4], \quad b_1 \subset [K_{z1}^L, K_{z1}^H],\ b_2 \subset [K_{z2}^L, K_{z2}^H],\ b_3 \subset [K_{\theta x1}^L, K_{\theta x1}^H],\ b_4 \subset [K_{\theta x2}^L, K_{\theta x2}^H] \tag{38}$$

where subscripts L and H denote the lower and upper bounds of clamp stiffness, respectively.

Considering the matrices in the equation of motion for the CPS as functions of the uncertain parameter vector, Eq. (8) can be rewritten as:

$$\boldsymbol{M}(\boldsymbol{b})\ddot{\boldsymbol{U}}(\boldsymbol{b}) + \boldsymbol{C}(\boldsymbol{b})\dot{\boldsymbol{U}}(\boldsymbol{b}) + \boldsymbol{K}(\boldsymbol{b})\boldsymbol{U}(\boldsymbol{b}) = \boldsymbol{F}(\boldsymbol{b}) \tag{39}$$

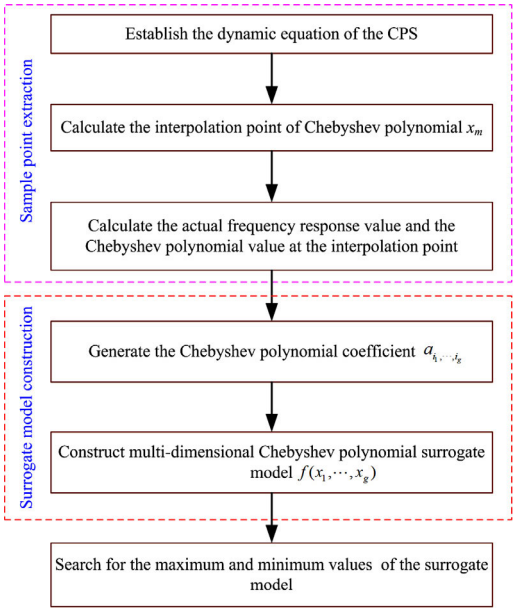

FIGURE 4. Calculation procedure for the CPS using the M-CPAM.

The interval of acceleration frequency response function of the excitation point $\hat{a}$ and the measurement point $\hat{b}$ is $H_a^{\hat{a}\hat{b}}(\omega) = \left[H_a^{\hat{a}\hat{b}}(\omega,\boldsymbol{b}), \bar{H}_a^{\hat{a}\hat{b}}(\omega,\boldsymbol{b})\right]$. The lower and upper bounds of the frequency response function can be expressed as:

$$H_a^{\hat{a}\hat{b}}(\omega,\boldsymbol{b}) = \min\left(\sum_{i=1}^{\bar{n}} \frac{-\omega^2 A_{\hat{a}i}(\boldsymbol{b})A_{\hat{b}i}(\boldsymbol{b})}{\omega_i(\boldsymbol{b})^2 + 2\xi_i\omega_i(\boldsymbol{b})\mathrm{j}\omega - \omega^2}\right) \tag{40}$$

$$\bar{H}_a^{\hat{a}\hat{b}}(\omega,\boldsymbol{b}) = \max\left(\sum_{i=1}^{\bar{n}} \frac{-\omega^2 A_{\hat{a}i}(\boldsymbol{b})A_{\hat{b}i}(\boldsymbol{b})}{\omega_i(\boldsymbol{b})^2 + 2\xi_i\omega_i(\boldsymbol{b})\mathrm{j}\omega - \omega^2}\right) \tag{41}$$

It is difficult to solve the interval range of the frequency response function directly. However, the Chebyshev polynomial surrogate model only needs a small number of original frequency response samples to calculate the approximate model at each frequency. Thus, the extreme values of the solutions (40) and (41) are transformed into the extreme values of the solutions (34). Based on the maximum value theorem for continuous function on a closed interval, the upper and lower bounds of the approximated function can be obtained by searching the maximum and minimum values of the multi-dimensional Chebyshev surrogate model f$(x_1,\cdots,x_g)$ on the standard interval [-1,1]. The calculation procedure for the CPS using the M-CPAM is shown in Fig. 4.

C. RESULTS COMPARISON

In this section, three uncertainty estimation methods will be compared. The mean of translational stiffness is taken as $K_{z1} = K_{z2} = 4.6 \times 10^6$N/m, and the mean of torsional stiffness is taken as $K_{\theta x1} = K_{\theta x2} = 55$ N·m/rad. The small uncertain level is assumed as the interval variable with 6.8 % uncertainty for the M-CPAM, which corresponds to a variable coefficient of 0.02 for the PCE and MCS. The larger uncertain

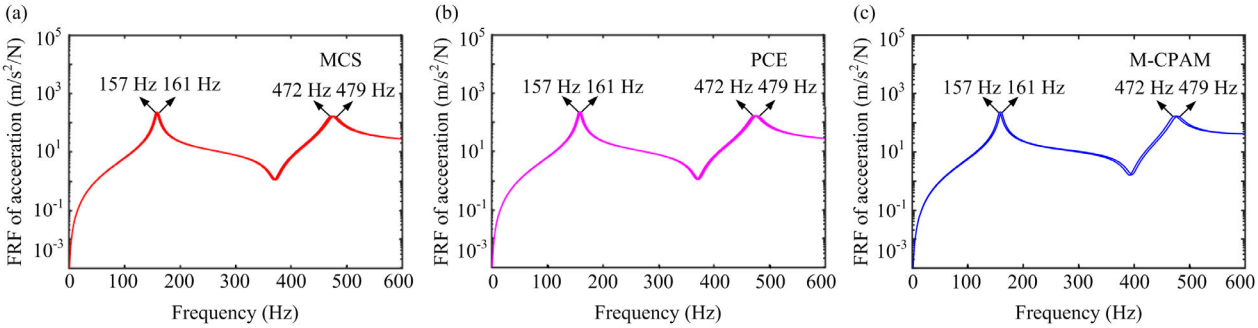

FIGURE 5. Comparison of three uncertainty estimation methods under small uncertain level: (a) MCS, (b) PCE, (c) M-CPAM.

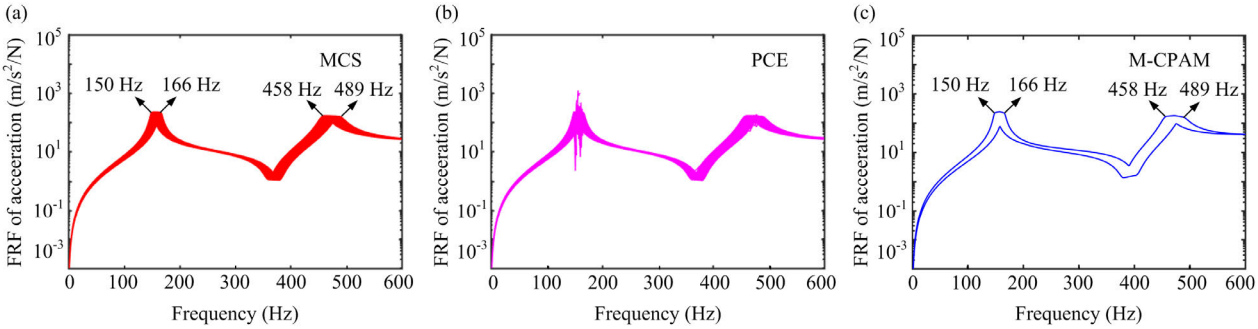

FIGURE 6. Comparison of three uncertainty estimation methods under larger uncertain level: (a) MCS, (b) PCE, (c) M-CPAM.

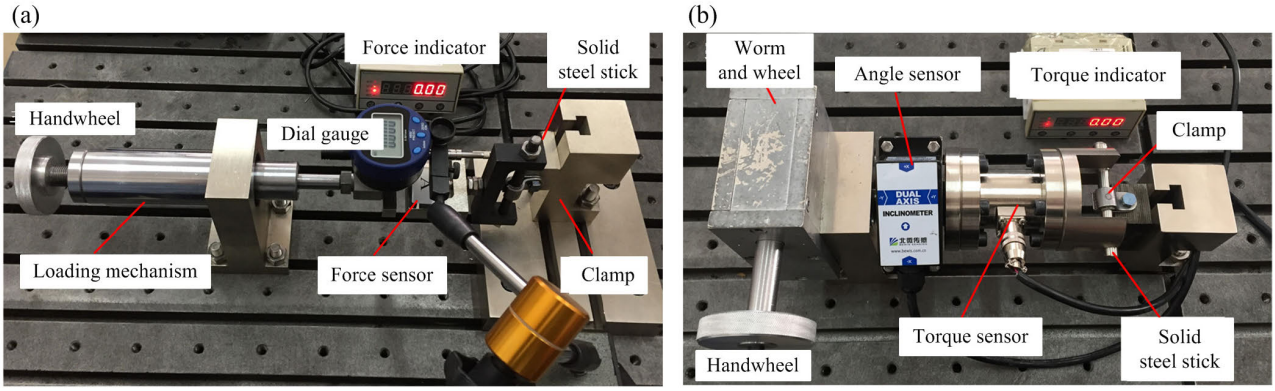

FIGURE 7. Test rig of clamp stiffness: (a) translational stiffness, (b) torsional stiffness.

level is assumed as the interval variable with 32% uncertainty for the M-CPAM, which corresponds to a variable coefficient of 0.1 for the PCE and MCS. Two examples under small uncertain level and the larger uncertain level are used to verify the proposed interval method. The calculations are performed using a personal computer with Intel Core i7-6700 3.40 GHz processor and 16 GB of RAM. The computing time using the MCS, PCE and M-CPAM is 650.6 s, 213.1 s and 101.8 s, respectively. And the results are depicted in Figs. 5 and 6.

The results of the three methods agree well in small uncertain level. However, in larger uncertain level, the PCE method will cause the amplitude oscillation in the resonance region (see Fig. 6(b)). This amplitude oscillation phenomenon caused by PCE also existed in Ref. [29]. The interval method still agrees well with MCS results (see Figs. 6(a) and (c)), which indicates that the applicability of the interval method is better. And the interval method provides a more accurate and time-saving and practical method for uncertainty analysis of CPS.

V. UNCERTAINTY ANALYSIS AND EXPERIMENTAL VERIFICATION OF THE FRF OF CPS

A. EXPERIMENTAL TEST

According to the results of sensitivity analysis in Section 2.2, the stiffness intervals of the clamp (K_z and $K_{\theta x}$) need to be measured. The test process is outlined as follows.

The self-designed clamp stiffness test rig is shown in Fig. 7. A complete test sequence includes forward loading, forward

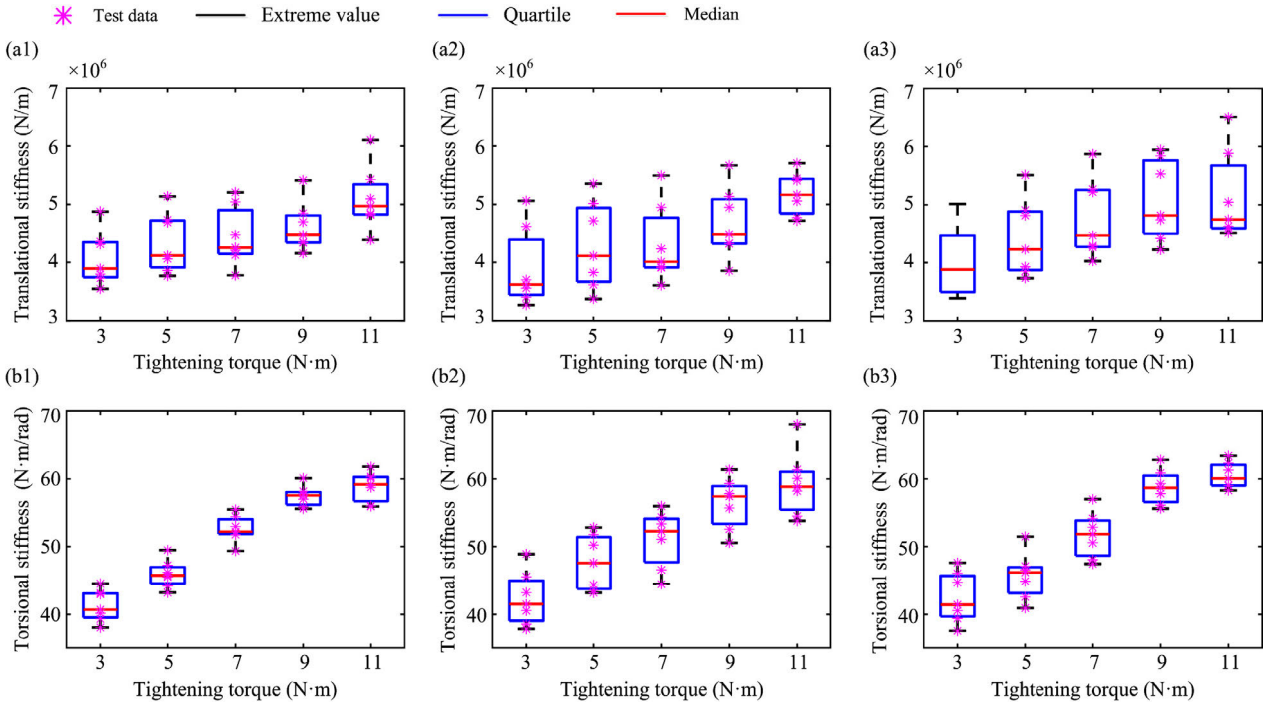

FIGURE 8. Test results of clamp 1: (a1-a3) translational stiffness data of K_{z1} for the first, second and third test, (b1-b3) torsional stiffness data of $K_{\theta x1}$ for the first, second and third test.

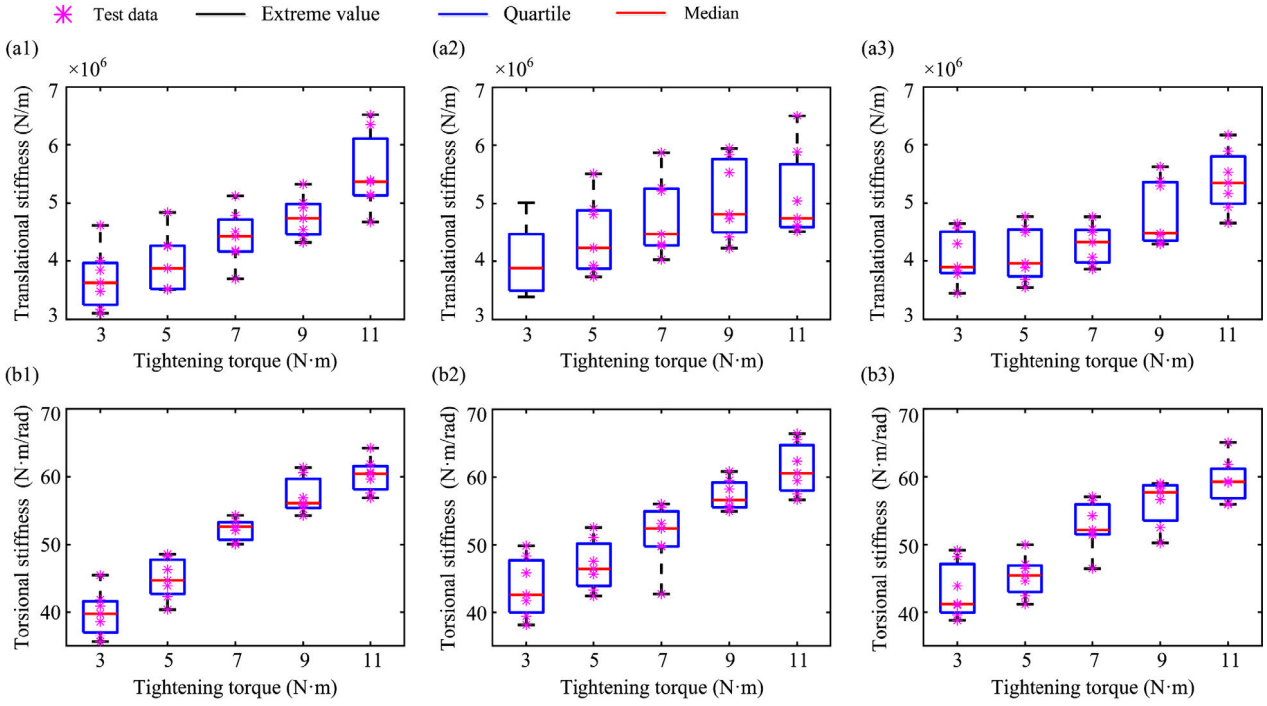

FIGURE 9. Test results of clamp 2: (a1-a3) translational stiffness data of K_{z2} for the first, second and third test, (b1-b3) torsional stiffness data of $K_{\theta x2}$ for the first, second and third test.

unloading, reverse loading, and reverse unloading. In the experiment, the loading shaft slowly moves forward or backward by rotating the handwheel, the force transducer is subjected to compression or tension, and finally the displacement is applied to the clamp. To be specific, the loading and unloading process is realized through threaded parts and

TABLE 1. Summary of test results.

Tightening torque of bolt (N • m)		3	5	7	9	11
Translational stiffness of clamp 1 K_{z1} (MN/m)	Minimum	3.2677	3.3728	3.6041	3.8550	4.3847
	Maximum	5.0621	5.5093	5.8747	5.9438	6.5076
	Standard deviation ($\times 10^6$)	0.5411	0.5727	0.5762	0.5325	0.5181
Translational stiffness of clamp 2 K_{z2} (MN/m)	Minimum	3.1039	3.5091	3.6935	4.1616	4.3366
	Maximum	4.8761	4.9405	5.1231	5.6216	6.5193
	Standard deviation ($\times 10^6$)	0.5001	0.4421	0.3840	0.3784	0.5486
Torsional stiffness of clamp 1 $K_{\theta x1}$ (N • m/rad)	Minimum	37.5876	40.9196	44.4385	50.5546	53.8020
	Maximum	48.8876	52.8236	56.9897	62.8036	68.0113
	Standard deviation ($\times 10$)	0.3034	0.2931	0.2945	0.2417	0.2733
Torsional stiffness of clamp 2 $K_{\theta x2}$ (N • m/rad)	Minimum	35.6156	40.3734	42.6827	50.2499	55.9479
	Maximum	49.8705	52.5667	57.0584	61.3497	66.4140
	Standard deviation ($\times 10$)	0.3686	0.3015	0.2999	0.2596	0.2910

TABLE 2. Comparison of simulation and experimental results under the same tightening torques of bolts on both sides.

Tightening torques of bolts (N • m)	Experiment of f_{n1} (Hz)	Experiment of f_{n2} (Hz)	lower bound error of f_{n1} (%)	upper bound error of f_{n1} (%)	lower bound error of f_{n2} (%)	upper bound error of f_{n2} (%)
3	139.3-152.4	435.3-458.4	4.1	2.3	3.8	3.0
5	148.5-158.5	447.5-460.6	0.3	0.3	1.7	2.5
7	160.9-169.2	462.2-482.2	6.8	5.4	0.7	1.1
9	165.3-168.3	477.9-479.5	7.4	3.7	2.9	0.1
11	168.2-170.1	482.2-484.5	7.8	3.0	2.9	0.5

TABLE 3. Comparison of simulation and experimental results under the same tightening torques of bolts on both sides.

Tightening torques of bolts (N • m)	Experiment of f_{n1} (Hz)	Experiment of f_{n2} (Hz)	lower bound error of f_{n1} (%)	upper bound error of f_{n1} (%)	lower bound error of f_{n2} (%)	upper bound error of f_{n2} (%)
T_L= 3, T_R= 5	151.4-156.3	433.4-460.8	2.9	0.4	4.8	2.4
T_L= 9, T_R= 5	161.1-163.6	453.6-456.9	6.9	2.2	1.2	4.2
T_L= 11, T_R= 3	156.9-159.1	447.2-450.8	4.4	0.6	2.6	6.0
T_L= 11, T_R= 9	164.5-173.4	479.7-481.3	5.8	6.0	2.6	0.4

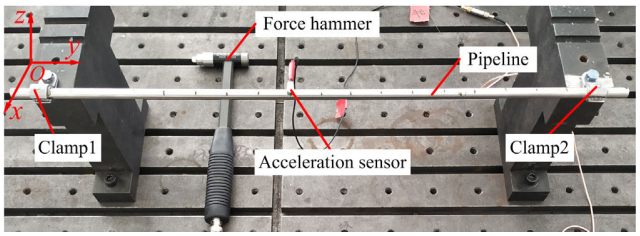

FIGURE 10. Hammering test rig.

controlled by internal spring support. To avoid gaps during loading and unloading, the forward and backward distance of the handwheel is amplified by the spring. The force sensor is connected to the two-end structure through the bolt of M8, and the force indicator can display the value of the tension pressure in real time. The displacement of clamp is measured by the dial gauge (see Fig. 7(a)). As for the angular stiffness test, worm drive loading method is applied to load torque accurately (see Fig. 7(b)). The angle sensor adopts BWL326 tilt angle sensor with a resolution of 0.01° and a measurement range of ±90°, which could meet the requirements of the experiment.

The translational stiffness in the z-direction and the torsional stiffness in the θ_x-direction are expressed as:

$$K_z = \Delta F_z / \Delta z K_{\theta x} = \Delta T_x / \Delta \theta_x \tag{42}$$

where ΔF_z and Δz represent the variation of the loading force and displacement in the z-direction. ΔT_x and $\Delta \theta_x$ denote the variation of the torque and angular displacement in the θ_x direction.

In order to facilitate the analysis of the influence of tightening torque on the CPS, the stiffness intervals of the clamp under 5 tightening torques (3 N·m, 5 N·m, 7 N·m, 9 N·m and 11 N·m) will be given here. The stiffness interval test process consists of three times disassembly and reassembly of the clamp. Once the clamp is reassembled, 7 complete tests should be completed under each tightening torque. The loading force and displacement data, torque and angular displacement data should be recorded at each test (The test data will not be shown here owing to space constraints). Substituting these data into the Eq. (42), the stiffness test results are shown in Figs. 8 and 9. The detailed calibration process of clamp stiffness can be found in Ref. [51].

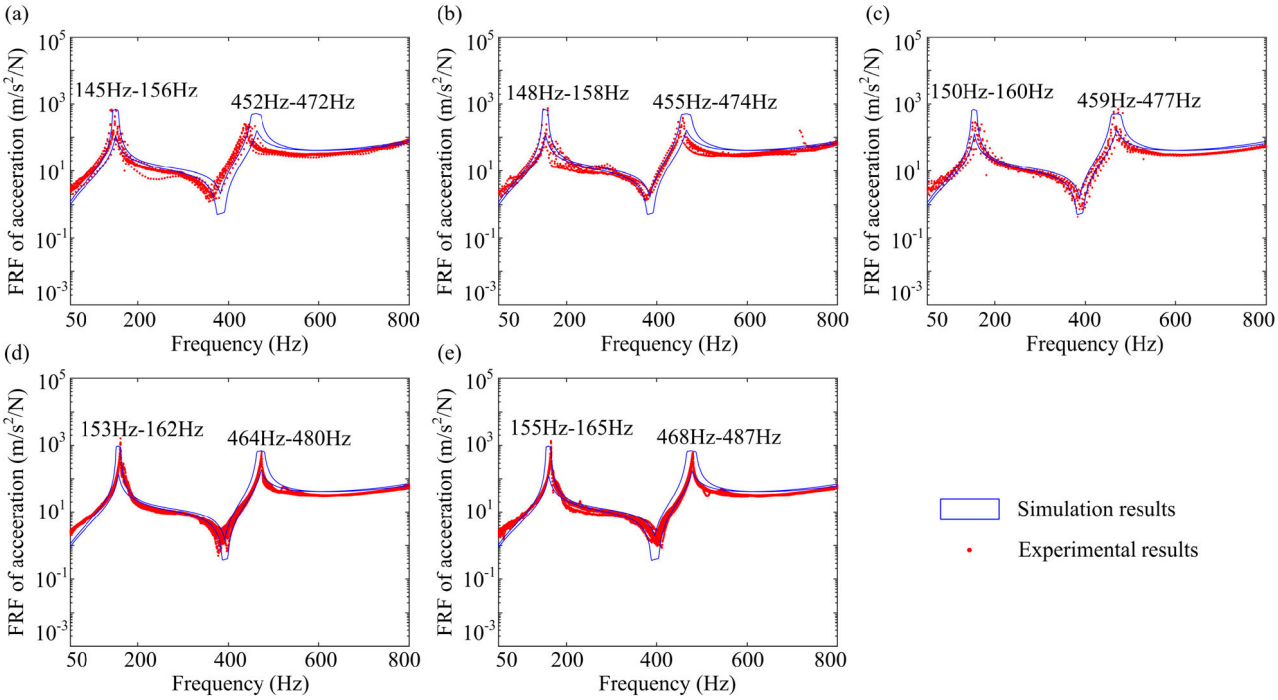

FIGURE 11. The FRF of simulation and experiment with uncertain stiffness parameters under the same tightening torques of bolts on both sides: (a) 3 N·m, (b) 5 N·m, (c) 7 N·m, (d) 9 N·m, (e) 11 N·m.

A box plot that commonly used in statistics is adopted to describe stiffness intervals of the clamp. In each group of test results, the pink point is the test data of the clamp stiffness under different tightening torques of the bolt. The black upper and lower bounds are the extreme values of the test data. The blue upper and lower bounds are the quartiles of the test data. The red line is the median of the test data. The maximum value, minimum value, and the standard deviation of the test data are shown in Table 1. Some conclusions can be summarized as follows:

(1) With the increase of tightening torque, the rate of change of the average value of $K_{\theta x}$ is greater than that of K_z (see Figs. 8 and 9).

(2) The standard deviations of the stiffness data show that the clamp stiffness has great dispersion under the same tightening torque. And the dispersion of K_z is greater than that of $K_{\theta x}$ (see Table 1).

(3) In this study, the maximum translational stiffness is about 1.6 times the minimum translational stiffness (clamp1 under the tightening torque of 7 N·m). And the maximum torsional stiffness is about 1.4 times the minimum torsional stiffness (clamp2 under the tightening torque of 3 N·m). Therefore, it is necessary to study the effects of stiffness uncertainty on frequency response.

For the sake of illustration, this section will briefly describe the hammering test (see Fig 10) for obtaining the frequency response data of the experiment in Section 4.2. A unidirectional lightweight acceleration sensor (CA-YD-125, mass 1.5 g) is adopted to reduce the effect of additional mass on the natural frequency of the pipeline. The type of impact hammer is PCB086C01. The response data of the experiment are collected by the LMS front-end controller. The node coordinates of knocking point are (0, 0.075, 0), and the node coordinates of the acceleration sensor are (0, 0.225, 0).

B. UNCERTAINTY ANALYSIS UNDER THE SAME TIGHTENING TORQUES OF BOLTS ON BOTH SIDES

Considering the influence of reassembly in the process of experiment, the clamp is reassembled every three groups of tests. The intervals of the frequency response are obtained by combining nine groups of experimental data. During the experiment, when measuring the frequency response of the CPS, a weak peak was found in the low-frequency region (0Hz-50Hz). This is because the acceleration sensor has a weak signal before the input pulse signals, which is considered to be a hardware problem of the test system. In order to eliminate such interference, the 50Hz-800Hz frequency band is intercepted for analysis when comparing the simulation results with the experimental results.

Taking the intervals of translational stiffness K_z and torsional stiffness $K_{\theta x}$ (see Table 1) as uncertain variables, the proposed M-CPAM is adopted to calculate the interval of the FRF of the CPS under the same tightening torques of bolts on both sides. The simulation and experimental results are shown in Fig 11 and Table 2.

Generally, the simulation results agree well with the experimental results, and the maximum error occurs at 11 N·m is 7.8%. One of the reasons for the error between simulation and experiment may be that the clamp containing metal rubber has been tightened and loosened many times. The mechanical

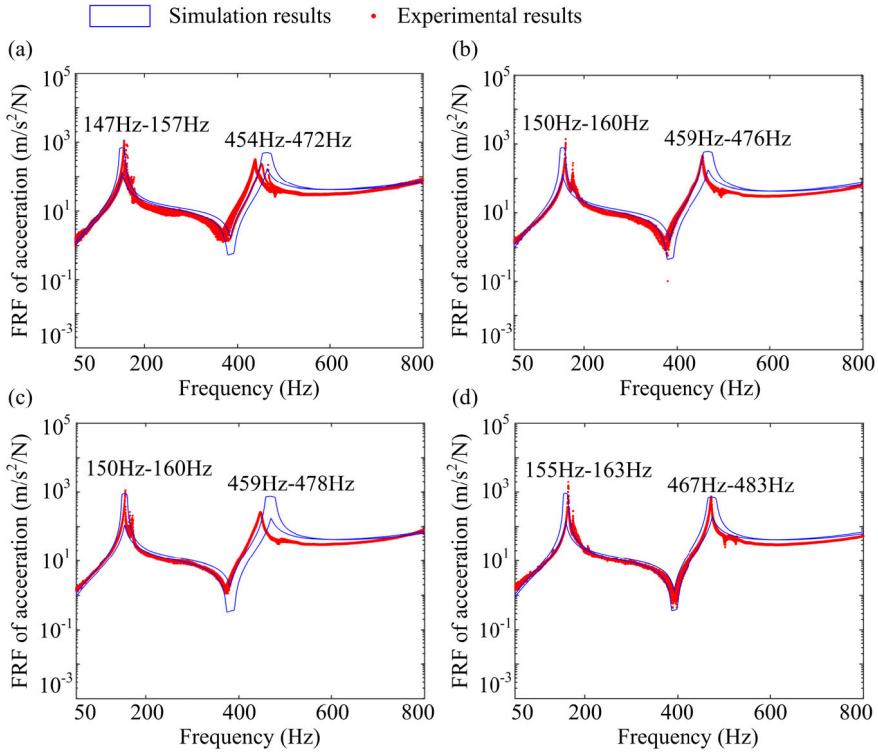

FIGURE 12. The FRF of simulation and experiment with uncertain stiffness parameters under the different tightening torques of bolts on both sides: (a) $T_L = 3$ N·m, $T_R = 5$ N·m, (b) $T_L = 9$ N·m, $T_R = 5$ N·m, (c) $T_L = 11$ N·m, $T_R = 3$ N·m, (d)$T_L = 11$N·m, $T_R = 9$ N·m.

properties of the clamp may deteriorate somewhat when the hammering test is carried out. Thus, the stiffness interval of the clamp during the hammering experiment is not completely consistent with the original measured stiffness interval of the clamp, resulting in errors.

It can be seen in Fig 11 that uncertainties have a significant influence on the dynamic response of CPS. With the increase of tightening torques, the interval values of the first-order and second-order natural frequency of the CPS gradually increase, which is a recognized frequency shift phenomenon. The amplitude at the resonance increases with the increase of tightening torques. It can be also seen that with the increase of tightening torque, the dispersion of frequency responses of simulation results tends to be concentrated except at 11 N·m (see Figs 11(a) and (d)). The possible reason is that after the tightening torque increases to a certain extent, the test results of the clamp stiffness interval is no longer accurate, leading to the deviation of simulation results. Compared with the experiment, the simulation results still have some overestimation in the resonance region. However, controlling the wrapping effect has always been the goal of uncertain estimation. In the future research, interval algorithm should be further improved to narrow the gap between experiment and simulation.

C. UNCERTAINTY ANALYSIS UNDER THE DIFFERENT TIGHTENING TORQUES OF BOLTS ON BOTH SIDES

In the actual engineering practice, the tightening torques of clamps on both sides of the pipeline may not be identical. In order to consider the influence of such factors, this section will conduct uncertainty analysis of the FRF of the CPS under the different tightening torques of bolts on both sides. Tightening torques of the left bolt and right bolt are defined as T_L and T_R. The simulation and experimental results are shown in Fig 12 and Table 3.

In Figs 12(b) and (c), the average tightening torque of bolts on both sides is 7 N·m. By comparing these two cases with the case under the same tightening torques (see Fig 11(c)), it can be seen that the frequency interval (150Hz-160Hz, 459Hz-477Hz) of the resonance region is basically close in the three cases. Therefore, to a certain extent, when the tightening torque of bolts on both sides is different, the average tightening torque can be used to approximate the uncertain interval of the FRF of CPS. It is worth pointing out that under some working conditions (Fig 12(c)), the amplitudes of simulation and experiment are not consistent, which may be caused by the excessive difference of tightening torque between the left and right sides of the pipeline during the experiment. On the whole, the experimental and simulation results are in good agreement, which further verifies the correctness of the proposed method. That is to say, the proposed M-CPAM for estimating the interval of the FRF of the CPS is desirable.

VI. CONCLUSION

For the clamp containing metal rubber layer, the stiffness uncertainty exists naturally in engineering. In this paper, the intervals of the clamp stiffness under different tightening

torques are measured by a self-designed test rig. Based on the measured data, a non-intrusive multi-dimensional Chebyshev polynomial approximation method (M-CPAM) is proposed to evaluate the uncertain characteristics of frequency response function (FRF) of clamp-pipeline system (CPS) caused by the uncertainty of the clamp stiffness. The superiority and effectiveness of the proposed method are verified by comparing with the results obtained from the Monte Carlo simulation (MCS), the experimental measurements, and the polynomial chaos expansion (PCE). The results show that the proposed method provides a more accurate, time-saving and practical method for solving the uncertainty of FRF of CPS. Some conclusions based on the current study are summarized as follows:

The clamp stiffness has great dispersion under the same tightening torque. Moreover, the dispersion of the translational stiffness K_z is greater than that of the torsional stiffness $K_{\theta x}$. For this paper, the maximum translational stiffness is about 1.6 times the minimum translational stiffness. And the maximum torsional stiffness is about 1.4 times the minimum torsional stiffness.

The frequency shift phenomenon will be observed in the resonance region of CPS when the clamp stiffness is uncertain. As the tightening torque increases from 3 N·m to 9 N·m, the dispersion of frequency responses of tends to be concentrated.

Compared with the experimental results, the simulation results still has some overestimation in the resonance region. In our future works, interval algorithm will be further improved to reduce the wrapping effect. Fluid effects during modeling and frequency response in other directions during testing will also be considered in the future study.

REFERENCES

[1] L. Yongshou, H. Xindang, Z. Youhai, and Y. Zhufeng, "Dynamical strength and design optimization of pipe-joint system under pressure impact load," *Proc. Inst. Mech. Eng. G, J. Aerosp. Eng.*, vol. 226, no. 8, pp. 1029–1040, Aug. 2012.

[2] A. A. Troynikov and K. V. Boyarov, "Mathematical model of cyclic loading of material MR," *ARPN J. Eng. Appl. Sci.*, vol. 9, no. 12, pp. 2890–2893, 2014.

[3] X. D. Kong, Y. Cao, L. X. Quan, and D. Li, "Research on natural vibration characteristic of metal pipelines with different length," in *Proc. IEEE/ASME Int. Conf. Adv.*, Aug. 2015, pp. 94–98.

[4] A. Tijsseling, "Water hammer with fluid-structure interaction in thick-walled pipes," *Comput. Struct.*, vol. 85, nos. 11–14, pp. 844–851, Jun. 2007.

[5] J. H. You and K. Inaba, "Fluid-structure interaction in water-filled thin pipes of anisotropic composite materials," *J. Fluids Struct.*, vol. 36, no. 7, pp. 162–173, 2013.

[6] P.-X. Gao, J.-Y. Zhai, Y.-Y. Yan, Q.-K. Han, F.-Z. Qu, and X.-H. Chen, "A model reduction approach for the vibration analysis of hydraulic pipeline system in aircraft," *Aerosp. Sci. Technol.*, vol. 49, pp. 144–153, Feb. 2016.

[7] P.-X. Gao, J.-Y. Zhai, F.-Z. Qu, and Q.-K. Han, "Vibration and damping analysis of aerospace pipeline conveying fluid with constrained layer damping treatment," *Proc. Inst. Mech. Eng. G, J. Aerosp. Eng.*, vol. 232, no. 8, pp. 1529–1541, Jun. 2018.

[8] P.-X. Gao, J.-Y. Zhai, and Q.-K. Han, "Dynamic response analysis of aero hydraulic pipeline system under pump fluid pressure fluctuation," *Proc. Inst. Mech. Eng. G, J. Aerosp. Eng.*, vol. 233, no. 5, pp. 1585–1595, Apr. 2019.

[9] H. Shen, J. Wen, D. Yu, and X. Wen, "The vibrational properties of a periodic composite pipe in 3D space," *J. Sound Vibrat.*, vol. 328, nos. 1–2, pp. 57–70, Nov. 2009.

[10] A. Ulanov and S. Bezborodov, "Research of stress-strained state of pipelines bundle with damping support made of MR material," *Procedia Eng.*, vol. 206, pp. 3–8, Jan. 2017.

[11] S. Bezborodov and A. Ulanov, "Calculation of vibration of pipeline bundle with damping support made of MR material," *Procedia Eng.*, vol. 176, pp. 169–174, Jan. 2017.

[12] R. Firouz-Abadi, M. Noorian, and H. Haddadpour, "A fluid–structure interaction model for stability analysis of shells conveying fluid," *J. Fluids Struct.*, vol. 26, no. 5, pp. 747–763, Jul. 2010.

[13] L. Quan, J. Gao, C. Guo, S. Wu, and J. Yao, "Dynamic model and response analysis of bionic hydraulic pipeline based on vascular physiological structure," *IEEE Access*, vol. 7, pp. 67564–67575, 2019.

[14] Q. Zhang, X. Kong, Z. Huang, B. Yu, and G. Meng, "Fluid-structure-interaction analysis of an aero hydraulic pipe considering friction coupling," *IEEE Access*, vol. 7, pp. 26665–26677, 2019.

[15] Q. Liu and G. Jiao, "A pipe routing method considering vibration for aero-engine using Kriging model and NSGA-II," *IEEE Access*, vol. 6, pp. 6286–6292, 2018.

[16] C. Ai, W. Bai, T. Zhang, and X. Kong, "Active control of pressure resonance in long pipeline of bottom founded hydraulic wind turbines based on multi-objective genetic algorithm," *IEEE Access*, vol. 6, pp. 53368–53380, 2018.

[17] Y. Ma, Q. Zhang, D. Zhang, F. Scarpa, B. Liu, and J. Hong, "The mechanics of shape memory alloy metal rubber," *Acta Mater.*, vol. 96, pp. 89–100, Sep. 2015, doi: 10.1016/j.actamat.2015.05.031.

[18] D. Zhang, F. Scarpa, Y. Ma, K. Boba, J. Hong, and H. Lu, "Compression mechanics of nickel-based superalloy metal rubber," *Mater. Sci. Eng., A*, vol. 580, pp. 305–312, Sep. 2013.

[19] G. Lazutkin, K. V. Boyarov, D. P. Davydov, T. V. Volkova, and L. A. Varzhitckii, "Design of elastic-damping supports made of MR material for pipeline supports," *Procedia Eng.*, vol. 176, pp. 326–333, Jan. 2017.

[20] C. Fu, X. Ren, Y. Yang, and W. Qin, "Dynamic response analysis of an overhung rotor with interval uncertainties," *Nonlinear Dyn.*, vol. 89, no. 3, pp. 2115–2124, Aug. 2017.

[21] D. Xiu and G. Em Karniadakis, "Modeling uncertainty in steady state diffusion problems via generalized polynomial chaos," *Comput. Methods Appl. Mech. Eng.*, vol. 191, no. 43, pp. 4927–4948, Sep. 2002.

[22] D. Xiu and G. E. Karniadakis, "Modeling uncertainty in flow simulations via generalized polynomial chaos," *J. Comput. Phys.*, vol. 187, no. 1, pp. 137–167, May 2003.

[23] M. Xu, J. Du, C. Wang, and Y. Li, "Hybrid uncertainty propagation in structural-acoustic systems based on the polynomial chaos expansion and dimension-wise analysis," *Comput. Methods Appl. Mech. Eng.*, vol. 320, pp. 198–217, Jun. 2017.

[24] X. Wan and G. E. Karniadakis, "An adaptive multi-element generalized polynomial chaos method for stochastic differential equations," *J. Comput. Phys.*, vol. 209, no. 2, pp. 617–642, Nov. 2005.

[25] A. Manan and J. Cooper, "Prediction of uncertain frequency response function bounds using polynomial chaos expansion," *J. Sound Vib.*, vol. 329, no. 16, pp. 3348–3358, Aug. 2010.

[26] T. Ritto, C. Soize, F. Rochinha, and R. Sampaio, "Dynamic stability of a pipe conveying fluid with an uncertain computational model," *J. Fluids Struct.*, vol. 49, pp. 412–426, Aug. 2014.

[27] S. Schmelter, A. Fiebach, R. Model, and M. Bär, "Numerical prediction of the influence of uncertain inflow conditions in pipes by polynomial chaos," *Int. J. Comput. Fluid Dyn*, vol. 29, nos. 6–8, pp. 411–422, Jul. 2015.

[28] E. Jacquelin, M. Friswell, S. Adhikari, O. Dessombz, and J.-J. Sinou, "Polynomial chaos expansion with random and fuzzy variables," *Mech. Syst. Signal Process.*, vol. 75, pp. 41–56, Jun. 2016.

[29] J.-J. Sinou and E. Jacquelin, "Influence of polynomial chaos expansion order on an uncertain asymmetric rotor system response," *Mech. Syst. Signal Process.*, vols. 50–51, pp. 718–731, Jan. 2015.

[30] Q. Liu, X. Zhang, and X. Huang, "A sparse surrogate model for structural reliability analysis based on the generalized polynomial chaos expansion," *Proc. IMechE O, J. Risk Rel.*, vol. 233, no. 3, pp. 487–502, Jun. 2019.

[31] X. Zhang and M. D. Pandey, "An effective approximation for variance-based global sensitivity analysis," *Rel. Eng. Syst. Saf.*, vol. 121, pp. 164–174, Jan. 2014.

[32] G. Dundulis, I. Žutautaitė, R. Janulionis, E. Ušpuras, S. Rimkevičius, and M. Eid, "Integrated failure probability estimation based on structural integrity analysis and failure data: Natural gas pipeline case," *Rel. Eng. Syst. Saf.*, vol. 156, pp. 195–202, Dec. 2016.
[33] H.-F. Duan, "Uncertainty analysis of transient flow modeling and transient-based leak detection in elastic water pipeline systems," *Water Resour. Manage.*, vol. 29, no. 14, pp. 5413–5427, Nov. 2015.
[34] M. Ahammed and R. Melchers, "Probabilistic analysis of pipelines subjected to pitting corrosion leaks," *Eng. Struct.*, vol. 17, no. 2, pp. 74–80, Feb. 1995.
[35] D. H. Rouvray, "Fuzzy sets and fuzzy logic: Theory and applications," *Control Eng. Pract.*, vol. 4, no. 9, pp. 1332–1333, 1996.
[36] A. Klimke, K. Willner, and B. Wohlmuth, "Uncertainty modeling using fuzzy arithmetic based on sparse grids: Applications to dynamic systems," *Int. J. Uncertainty, Fuzziness Knowl.-Based Syst.*, vol. 12, no. 6, pp. 745–759, Dec. 2004.
[37] A. Klimke and B. Wohlmuth, "Computing expensive multivariate functions of fuzzy numbers using sparse grids," *Fuzzy Sets Syst.*, vol. 154, no. 3, pp. 432–453, Sep. 2005.
[38] V. Puig, J. Saludes, and J. Quevedo, "Simulation of discrete linear time-invariant fuzzy dynamic systems," *Fuzzy Sets Syst.*, vol. 159, no. 7, pp. 787–803, Apr. 2008.
[39] R. Revelli and L. Ridolfi, "Fuzzy approach for analysis of pipe networks," *J. Hydraul. Eng.*, vol. 128, no. 1, pp. 93–101, Jan. 2002.
[40] Z. Qiu and X. Wang, "Comparison of dynamic response of structures with uncertain-but-bounded parameters using non-probabilistic interval analysis method and probabilistic approach," *Int. J. Solids Struct.*, vol. 40, no. 20, pp. 5423–5439, Oct. 2003.
[41] J. Wu, Y. Zhang, L. Chen, and Z. Luo, "A Chebyshev interval method for nonlinear dynamic systems under uncertainty," *Appl. Math. Model.*, vol. 37, no. 6, pp. 4578–4591, Mar. 2013.
[42] J. Wu, Z. Luo, Y. Zhang, N. Zhang, and L. Chen, "Interval uncertain method for multibody mechanical systems using Chebyshev inclusion functions," *Int. J. Numer. Method Engng*, vol. 95, no. 7, pp. 608–630, Aug. 2013.
[43] J. Wu, Z. Luo, N. Zhang, and Y. Zhang, "A new interval uncertain optimization method for structures using Chebyshev surrogate models," *Comput. Struct.*, vol. 146, pp. 185–196, Jan. 2015.
[44] J. Wu, Z. Luo, N. Zhang, and Y. Zhang, "A new uncertain analysis method and its application in vehicle dynamics," *Mech. Syst. Signal Process.*, vols. 50–51, pp. 659–675, Jan. 2015.
[45] C. Fu, X. Ren, and Y. Yang, "Vibration analysis of rotors under uncertainty based on Legendre series," *J. Vib. Eng. Technol.*, vol. 7, no. 1, pp. 43–51, Feb. 2019.
[46] C. Fu, X. Ren, Y. Yang, Y. Xia, and W. Deng, "An interval precise integration method for transient unbalance response analysis of rotor system with uncertainty," *Mech. Syst. Signal Process.*, vol. 107, pp. 137–148, Jul. 2018.
[47] G. Muscolino, R. Santoro, and A. Sofi, "Explicit frequency response functions of discretized structures with uncertain parameters," *Comput. Struct.*, vol. 133, pp. 64–78, Mar. 2014.
[48] Y. Yaowen, C. Zhenhan, and L. Yu, "Interval analysis of frequency response functions of structures with uncertain parameters," *Mech. Res. Commun.*, vol. 47, pp. 24–31, Jan. 2013.
[49] M. W. Lesmez, *Modal Analysis of Vibrations in Liquid-filled Piping System*. East Lansing, MI, USA: Michigan State Univ., 1989.
[50] G. Mikota, "Modal analysis of hydraulic pipelines," *J. Sound Vib.*, vol. 332, no. 16, pp. 3794–3805, Aug. 2013.
[51] Q. D. Chai, Y. H. Piao, H. Ma, W. X. Wu, and W. Sun, "Calculation of natural characteristics and experimental methods of the clamp-pipe system," (in Chinese), *J. Aerosp. Power*, vol. 34, no. 5, pp. 1029–1035, 2019.

XUMIN GUO was born in Hebei, China, in 1992. He received the B.S. degree in mechanical engineering from Ludong University, Yantai, China, in 2016. He is currently pursuing the master's degree in mechanical design and theory with Northeastern University. His research interest is mechanical dynamics.

HUI MA received the M.Sc. and Ph.D. degrees in mechanical engineering from Northeastern University, Shenyang, China, in 2004 and 2007, respectively.

He is currently a Professor with the School of Mechanical Engineering and Automation, Northeastern University. His research interests include dynamic modeling and fault diagnosis of rotating machinery, vibration characteristic analysis of rotating machinery, and machinery fault diagnosis. He is an editorial board member of *Advances in Mechanical Engineering*.

XUFANG ZHANG was born in Liaoning, China, in 1980. He received the Ph.D. degree from the University of Waterloo, Canada, in 2013. He is currently an Associate Professor with the School of Mechanical Engineering and Automation, Northeastern University, Shenyang, China. His research interest includes the probability quantization research and engineering application of complex mechanical structure.

ZHUANG YE was born in Hubei, China, in 1996. He received the B.S. degree in mechanical engineering from the Northeastern University of Mechanical Engineering, Liaoning, China, in 2018. He is currently pursuing the master's degree in mechanical engineering with Northeastern University. His research interest is mechanical dynamics.

QIANG FU was born in Liaoning, China, in 1995. He received the B.S. degree in mechanical engineering from the Hubei University of Automotive Technology, Shiyan, China, in 2018. He is currently pursuing the master's degree in mechanical design and theory with Northeastern University. His research interest is mechanical dynamics.

ZHONGHUA LIU was born in Liaoning, China, in 1988. He received the B.S. degree in mechanical engineering from Beihang University, Beijing, China, in 2017.

He is currently with the Shenyang Engine Research Institute. His research interest includes the piping design and dynamic analysis of aircraft engines.

QINGKAI HAN received the Ph.D. degree in mechanical engineering from Northeastern University, Shenyang, China, in 1997. His research interest includes mechanical dynamics and vibration.